Magnetic properties of the layered heavy-fermion antiferromagnet CePdGa6

H. Q. Ye, T. Le, H. Su, Y. N. Zhang, S. S. Luo, M. J. Gutmann, H. Q. Yuan, and M. Smidman

Magnetic properties of the layered heavy-fermion antiferromagnet CePdGa$_6$

H. Q. Ye,[1] T. Le,[1] H. Su,[1] Y. N. Zhang,[1] S. S. Luo,[1] M. J. Gutmann,[2] H. Q. Yuan,[1,3,4,5] and M. Smidman [1,3,*]

[1]*Center for Correlated Matter and Department of Physics, Zhejiang University, Hangzhou 310058, China*
[2]*ISIS Facility, Rutherford Appleton Laboratory, Chilton, Didcot Oxon OX11 0QX, United Kingdom*
[3]*Zhejiang Province Key Laboratory of Quantum Technology and Device, Department of Physics,*
Zhejiang University, Hangzhou 310058, China
[4]*State Key Laboratory of Silicon Materials, Zhejiang University, Hangzhou 310058, China*
[5]*Collaborative Innovation Center of Advanced Microstructures, Nanjing University, Nanjing 210093, China*

We report the magnetic properties of the layered heavy-fermion antiferromagnet CePdGa$_6$ and their evolution upon tuning with the application of magnetic field and pressure. CePdGa$_6$ orders antiferromagnetically below $T_N = 5.2$ K, where there is evidence for heavy-fermion behavior from an enhanced Sommerfeld coefficient. Our results are best explained by a magnetic ground state of ferromagnetically coupled layers of Ce $4f$ moments orientated along the c axis, with antiferromagnetic coupling between layers. At low temperatures, we observe two metamagnetic transitions for fields applied along the c axis corresponding to spin-flip transitions, where the lower transition is to a different magnetic phase with a magnetization one-third of the saturated value. From our analysis of the magnetic susceptibility, we propose a crystalline electric field level scheme which accounts for the Ising anisotropy at low temperatures, and we find that the evolution of the magnetic ground state can be explained considering both antiferromagnetic exchange between nearest neighbor and next-nearest neighbor layers, indicating the influence of long-range interactions. Meanwhile, we find little change of T_N upon applying hydrostatic pressures up to 2.2 GPa, suggesting that significantly higher pressures are required to examine for possible quantum critical behaviors.

I. INTRODUCTION

Heavy-fermion compounds are prototypical examples of strongly correlated electron systems and have been found to host a range of emergent phenomena including unconventional superconductivity, complex magnetic order, and strange metal behavior [1–3]. Ce-based heavy fermions contain a Kondo lattice of Ce ions with an unpaired $4f$ electron, which can both couple to other $4f$ moments via the Ruderman-Kittel-Kasuya-Yosida (RKKY) interaction and undergo the Kondo interaction due to hybridization with the conduction electrons. Here, the RKKY interaction gives rise to long-range magnetic order, while the Kondo interaction favors a nonmagnetic Fermi-liquid ground state with greatly enhanced quasiparticle masses. Due to the small energy scales, the relative strengths of these competing interactions can often be tuned by nonthermal parameters such as pressure, magnetic fields, and chemical doping [4], and in many cases, the magnetic ordering can be continuously suppressed to zero temperature at a quantum critical point (QCP).

A major question for heavy-fermion systems is the relationship between quantum criticality and the dome of unconventional superconductivity sometimes found to encompass the QCP. CeIn$_3$ is a canonical example of this phenomenon, which at ambient pressure orders antiferromag-netically below $T_N = 10.1$ K but exhibits a pressure-induced QCP at 2.6 GPa, which is surrounded by a superconducting dome with a maximum T_c of 0.2 K [5]. The layered CeMIn$_5$ (M = transition metal) compounds consist of alternating layers of MIn$_2$ and CeIn$_3$ along the c axis [6], and among the remarkable properties is a significantly enhanced superconducting T_c for the M = Rh and Co systems, reaching >2 K [7,8], giving a strong indication that quasi-two dimensionality is important for promoting heavy-fermion superconductivity. Meanwhile, the Ce$_2$$MIn_8$ compounds correspond to a stacked arrangement of two units of CeIn$_3$ and one of MIn$_2$ [9] and are expected to have an intermediate degree of two dimensionality relative to CeMIn$_5$. Correspondingly, the superconducting phases have lower T_c values of 0.4 and 0.68 K for Ce$_2$CoIn$_8$ [10] and Ce$_2$PdIn$_8$ [11] at ambient pressure and a maximum of $T_c = 2$ K at 2.3 GPa for Ce$_2$RhIn$_8$ [12]. On the other hand, these different series of related Ce-based heavy-fermion systems also exhibit different magnetic ground states and crystalline electric field (CEF) level schemes [13–17], and therefore, it is challenging to disentangle the role of these factors from that of the reduced dimensionality. The elucidation of the interplay between these different aspects requires examining additional families of layered Ce-based heavy-fermion systems for quantum critical behaviors as well as detailed characterizations of the magnetic ground states and exchange interactions.

The properties of layered Ce-based heavy-fermion gallides have been less studied than the indium-based systems. CeGa$_6$
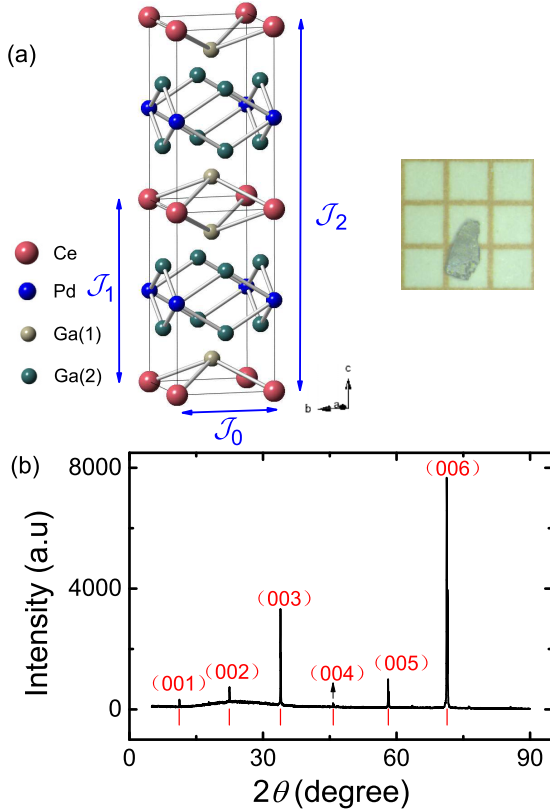

FIG. 1. (a) Crystal structure of $CePdGa_6$ where the red, blue, and green atoms correspond to Ce, Pd, and Ga, respectively. $\mathcal{J}_0$ represents magnetic exchange interactions between nearest neighbor Ce atoms within the *ab* plane, $\mathcal{J}_1$ is between nearest neighboring layers, and $\mathcal{J}_2$ is between next-nearest layers. An image of a typical single crystal of $CePdGa_6$ is also displayed, where each square in the background is 2×2 mm. (b) X-ray diffraction pattern measured on a single crystal of $CePdGa_6$. The red dashes correspond to the positions of the $(00l)$ Bragg peaks, indicating that the [001] direction is perpendicular to the large face of the platelike samples.

has a layered tetragonal structure (space group $P4/nbm$), with four Ga layers between each Ce layer [18]. This compound orders magnetically below $T_N = 1.7$ K, and there is evidence for the buildup of magnetic correlations at significantly higher temperatures [19]. A more layered structure is realized in the Ce_2MGa_{12} (M = Cu, Ni, Rh, Pd, Ir, or Pt) series, where the Ce layers are alternately separated by four Ga layers and units of MGa_6, leading to a larger interlayer separation of the Ce atoms [20,21]. Several members of this series show evidence for both antiferromagnetism and heavy-fermion behavior [20–25], where pressure can readily suppress the antiferromagnetic transitions of Ce_2NiGa_{12} and Ce_2PdGa_{12} [26,27], while evidence for field-induced critical fluctuations is revealed in Ce_2IrGa_{12} [25].

$CePdGa_6$ has a different layered tetragonal structure (space group $P4/mmm$) displayed in Fig. 1(a), consisting of square layers of Ce atoms, with each Ce contained in a $CeGa_4$ prism, separated by $PdGa_2$ layers [28]. Correspondingly, there is a distance between Ce layers of 7.92 Å, while the nearest neighbor in-plane Ce-Ce separation is 4.34 Å compared with respective values of 7.54 and 4.65 Å in $CeRhIn_5$ [29].

$CePdGa_6$ orders antiferromagnetically below $T_N = 5.2$ K, and heavy-fermion behavior is evidenced by an enhanced Sommerfeld coefficient [20,28]. As such, $CePdGa_6$ is a good candidate to look for behaviors arising in quasi-two-dimensional heavy-fermion systems, but there is both a lack of detailed characterizations of the magnetic ground state and no reports of the evolution under pressure. In addition, most measurements of $CePdGa_6$ are reported in Ref. [28], where the results are affected by the inclusion of an extrinsic antiferromagnetic phase Ce_2PdGa_{12}, which can be eliminated using a modified crystal growth procedure [20].

In this paper, we report detailed measurements of the magnetic properties of single crystals of $CePdGa_6$, including their evolution upon applying magnetic fields and hydrostatic pressure. We find that $CePdGa_6$ orders antiferromagnetically in zero field, where the Ce moments are orientated along the *c* axis and align ferromagnetically within the *ab* plane, but there is antiferromagnetic coupling between layers. At low temperatures, two metamagnetic transitions are observed for fields along the *c* axis, the lower of which corresponds to a spin-flip transition to a phase with magnetization one-third of the saturated value. From our analysis of the magnetic susceptibility, we propose a CEF level scheme which can explain the low-temperature Ising anisotropy, and we find that, from considering interactions between the nearest neighbor and next-nearest neighbor Ce layers, the field evolution of the magnetic state can be well accounted for.

II. EXPERIMENTAL DETAILS

Single crystals of $CePdGa_6$ were grown using a Ga self-flux method with a molar ratio of Ce : Pd : Ga of 1:1.5:15 [20]. Starting materials of Ce ingot (99.9%), Pd powder (99.99%), and Ga pieces (99.99%) were loaded into an alumina crucible which was sealed in an evacuated quartz tube. The tube was heated to 1150 °C and held at this temperature for 2 h before being rapidly cooled to 500 °C at a rate of 150 K/h and then cooled more slowly to 400 °C at 8 K/h. After being held at 400 °C for 2 wk, the tube was removed from the furnace and centrifuged to remove excess Ga. The obtained crystals were platelike with typical dimensions $2 \times 1.5 \times 0.3$ mm^3. Note that, when slower cooling rates of 6 or 4 K/h were used, the resulting crystals were significantly smaller. Single crystals of the nonmagnetic analog $LaPdGa_6$ were also obtained using a similar procedure. The composition was confirmed using a cold field emission scanning electron microscope (SEM) equipped with an energy dispersive x-ray spectrometer. The phase of the crystals was checked using both a PANalytical XPert MRD powder diffractometer using Cu-Kα radiation and a Rigaku-Oxford diffraction Xtalab synergy single-crystal diffractometer equipped with a HyPix hybrid pixel array detector using Mo-Kα radiation. The obtained lattice parameters from the single-crystal diffraction data of $a = 4.3446(3)$ Å and $c = 7.9173(10)$ Å are in excellent agreement with previous reports [28]. Measurements of a crystal using the powder diffractometer are displayed in Fig. 1(b), where all the Bragg peaks are well indexed by the $(00l)$ reflections of $CePdGa_6$, demonstrating that the *c* axis is perpendicular to the large face of the crystals. Resistivity and specific heat measurements were performed in applied fields up to 14 T using
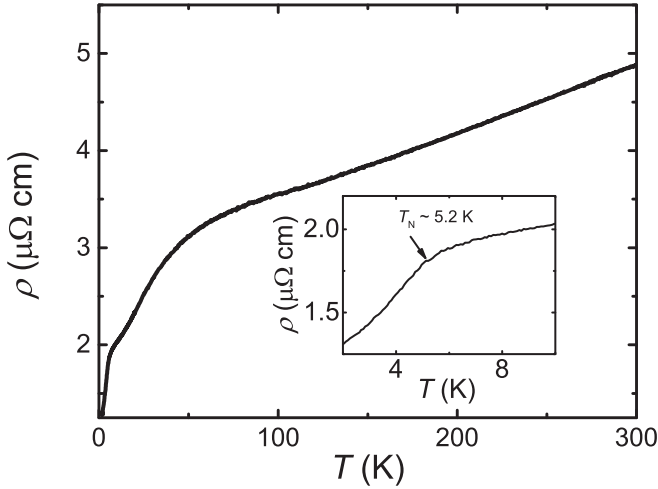
FIG. 2. Temperature dependence of the resistivity $\rho(T)$ of CePdGa6 between 1.8 and 300 K. The inset displays the low-temperature resistivity, where there is a sharp anomaly at the antiferromagnetic transition.

a Quantum Design Physical Property Measurement System (PPMS-14) down to 1.8 K and to 0.3 K using a ^{3}He insert. Resistivity measurements were performed after spot welding four Pt wires to the surface, with the excitation current in the *ab* plane. Magnetization measurements were performed in the range 1.8–300 K in applied fields up to 5 T using a Quantum Design Magnetic Property Measurement System (MPMS) superconducting quantum interference device magnetometer. Heat capacity measurements under pressure were carried out in a piston cylinder cell, using an ac calorimetric method.

III. RESULTS

A. Antiferromagnetic transition and CEF excitations of CePdGa6

Figure 2 displays the temperature dependence of the resistivity $\rho(T)$ of CePdGa6 between 1.8 and 300 K, which has a residual resistivity ratio $[\rho(300\,\mathrm{K})/\rho(2\,K)] = 3.8$. A broad shoulder is observed at ∼50 K, which likely arises due to both the Kondo effect and as a consequence of CEF excitations. At higher temperatures, quasilinear behavior is observed, which could be due to electron-phonon coupling. As shown in the inset, there is an anomaly at around $T_N = 5.2$ K, below which $\rho(T)$ decreases more rapidly with decreasing temperature, which corresponds to the antiferromagnetic transition reported previously [20], while no signature of the spurious transition at higher temperatures is detected [28]. The total specific heat of CePdGa6 and nonmagnetic isostructural LaPdGa6 are shown in the inset of Fig. 3(a). The temperature dependence of the magnetic contribution to the specific heat C_m was estimated by subtracting the data of LaPdGa6, which is shown in Fig. 3(a), while the specific heat coefficient C_m/T and the magnetic entropy S_m of CePdGa6 are displayed in Fig. 3(b). A pronounced λ-like anomaly is observed at $T_N = 5.2$ K, as is typical for a second-order magnetic phase transition. For $T > T_N$, C_m/T increases with decreasing
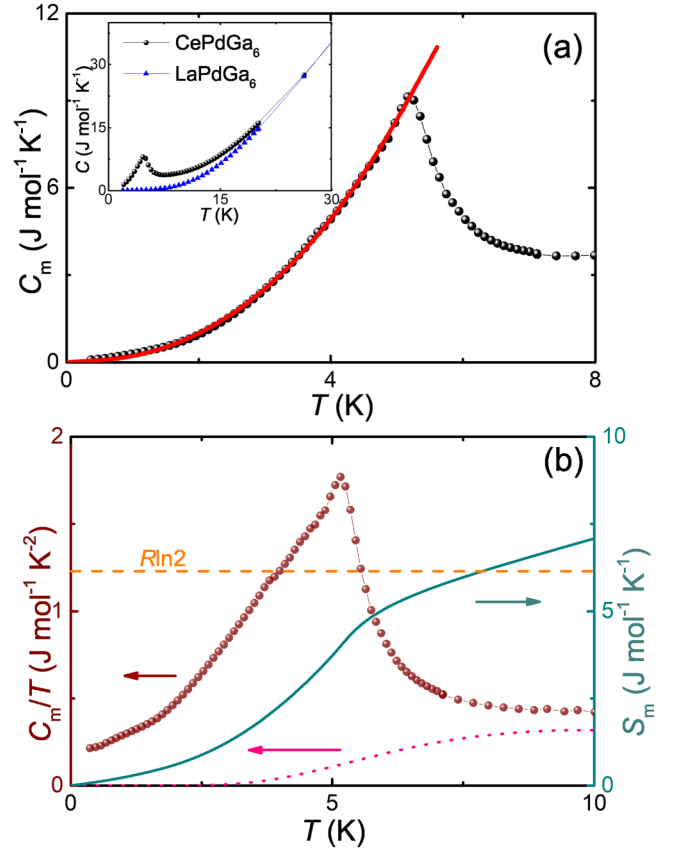

FIG. 3. (a) Magnetic contribution to the specific heat C_m at low temperatures, where the red solid line shows the results from fitting with Eq. (1). The inset shows the total specific heat C of CePdGa6 and the nonmagnetic analog LaPdGa6. (b) Temperature dependence of C_m/T and the magnetic entropy S_m of CePdGa6. The pink dotted line displays the low temperature contribution to the specific heat calculated from the crystalline electric field (CEF) scheme deduced from the analysis of $\chi(T)$.

temperature and extrapolates to a relatively large zero temperature value of $250\,\mathrm{mJ/mol\,K^2}$. As discussed below, the analysis of the magnetic susceptibility $\chi(T)$ suggests the presence of a low-lying CEF level, which could contribute to C_m/T in this temperature range. The dotted line in Fig. 3(b) shows the calculated C_m/T for the CEF level scheme described below, which has a sizable value in the vicinity of the transition. Subtracting the contribution from the CEF at T_N yields an estimate of $\gamma \sim 121.4\,\mathrm{mJ/mol\,K^2}$ associated with the ground state doublet, and such an enhanced value could arise both due to heavy-fermion behavior as well as the presence of short-range magnetic correlations, as inferred in CeRhIn5[30,31]. The data below T_N were analyzed using [32]

$$C_m = \gamma T + c\Delta_{SW}^{7/2}\sqrt{T}\exp\left(\frac{-\Delta_{SW}}{T}\right)$$
$$\times\left[1 + \frac{39T}{20\Delta_{SW}} + \frac{51}{32}\left(\frac{T}{\Delta_{SW}}\right)^2\right], \quad (1)$$

where the first term corresponds to the electronic contribution, and the second term arises due to antiferromagnetic spin-waves. Here, the coefficient c is related to the spin-wave
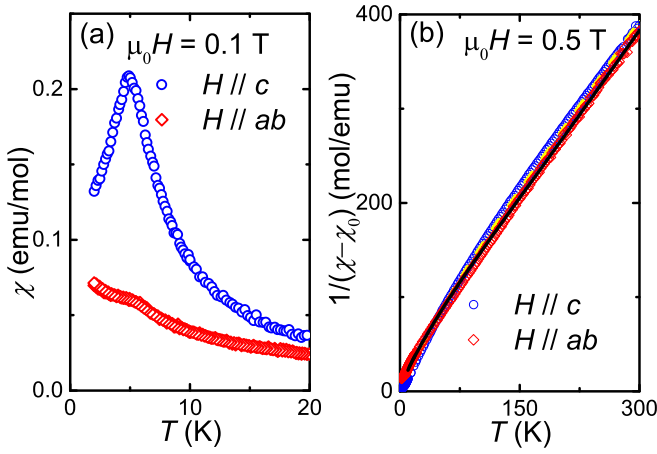
FIG. 4. (a) Low-temperature magnetic susceptibility $\chi(T)$ of CePdGa$_6$, with an applied field of $\mu_0 H = 0.1$ T both parallel to the c axis and within the ab plane. (b) Temperature dependence of $1/(\chi - \chi_0)$ up to 300 K for 0.5 T applied along the two field directions, where the dashed and solid lines show the results from fitting with the crystalline electric field (CEF) model described in the text.

stiffness D via $c \propto D^{-3}$, while Δ_{SW} is the spin-wave gap. The results from fitting the zero-field data are displayed in the main panel of Fig. 3(a), where $\gamma = 121.4$ mJ/mol K^2 was fixed, yielding $\Delta_{SW} = 2.3$ K and $c = 23$ mJ/mol K^2. The moderate value of Δ_{SW} is smaller than T_N, unlike the layered heavy-fermion gallides Ce$_2$PdGa$_{12}$ and Ce$_2$IrGa$_{12}$, where $\Delta_{SW} > T_N$ [24,25], likely reflecting the weaker magnetocrystalline anisotropy in CePdGa$_6$. The temperature dependence of the magnetic entropy S_m of CePdGa$_6$ is also displayed in Fig. 3(b), obtained by integrating C_m/T, where C_m/T was linearly extrapolated <0.4 K. At T_N, S_m reaches $0.76R \ln 2$, which together with the expected sizable contribution from the excited CEF level discussed above suggests a reduced entropy corresponding to the ground state doublet due to Kondo screening.

Figure 4(a) displays the temperature dependence of the magnetic susceptibility $\chi(T)$ of CePdGa$_6$ at low temperatures, with an applied field of $\mu_0 H = 0.1$ T along the c axis and within the ab plane, which both exhibit an anomaly at T_N. At low temperatures, $\chi(T)$ is significantly larger for fields along the c axis than in the ab plane, demonstrating that the c axis is the easy axis of magnetization. At T_N, there is a peak in $\chi(T)$ for $H \parallel c$, while for $H \parallel ab$, $\chi(T)$ weakly increases below T_N, indicating that this corresponds to an antiferromagnetic transition with moments ordered along the easy c axis.

At higher temperatures, the data >100 K can be analyzed using the Curie-Weiss law: $\chi = \chi_0 + C/(T - \theta_{CW})$, where χ_0 is a temperature-independent term, C is the Curie constant, and θ_{CW} is the Curie-Weiss temperature, yielding $\theta_{CW}^c = -11.7(3)$ K and an effective moment of $\mu_{eff}^c = 2.35\mu_B$/Ce for $H \parallel c$, as well as $\theta_{CW}^{ab} = -12.9(8)$ K and $\mu_{eff}^{ab} = 2.49\mu_B$/Ce for $H \parallel ab$. The obtained values of μ_{eff} for both directions are close to the full value of $2.54\,\mu_B$ for the $J = \frac{5}{2}$ ground state multiplet of Ce^{3+}. At lower temperatures, there is a deviation of $\chi(T)$ from Curie-Weiss behavior, due to the splitting of the ground state multiplet by crystalline-electric fields. To analyze the CEF level scheme, we considered the following

Hamiltonian for a Ce^{3+} ion in a tetragonal CEF [33]:

$$\mathcal{H}_{CF} = B_2^0 O_2^0 + B_4^0 O_4^0 + B_4^4 O_4^4, \quad (2)$$

where O_l^m and B_l^m are Stevens operator equivalents and parameters, respectively. The B_2^0 parameter can be estimated from the high-temperature susceptibility using [34]

$$B_2^0 = \frac{10k_B(\theta_{CW}^{ab} - \theta_{CW}^c)}{3(2J-1)(2J+3)}, \quad (3)$$

where $J = \frac{5}{2}$ for the ground state multiplet of Ce^{3+}, yielding $B_2^0 = -0.01077$ meV. Here, $\chi(T)$ along both directions was analyzed considering the contribution from the CEF χ_{CEF}^i as well as molecular field parameters λ^i using

$$\chi^i = \chi_0^i + \frac{\chi_{CEF}^i}{1 - \lambda^i \chi_{CEF}^i}, \quad (4)$$

where the superscript i denotes the c axis or ab plane. With B_2^0 fixed from Eq. (3), values of $B_4^0 = -0.0746$ meV and $|B_4^4| = 0.496$ meV were obtained, together with molecular field parameters of $\lambda^c = -3.55$ mol/emu and $\lambda^{ab} = 8.15$ mol/emu, $\chi_0^c = 2.2 \times 10^{-4}$ emu/mol and $\chi_0^{ab} = -2.3 \times 10^{-3}$ emu/mol, and the fitted results are shown in Fig. 4(b). These parameters yield a CEF scheme with a Γ_7 ground state Kramers doublet $|\psi_1^\pm\rangle = 0.883| \pm \frac{5}{2}\rangle - 0.469| \mp \frac{3}{2}\rangle$ (for positive B_4^4), and excitations to Γ_6 and Γ_7 levels of $\Delta_1 = 2.8$ meV and $\Delta_2 = 32.1$ meV, respectively. At high temperatures, the small negative B_2^0 leads to a nearly isotropic $\chi(T)$, while at low temperatures, the negative B_4^0 leads to the observed Ising anisotropy with an easy c axis. The predicted moment along the c axis is given by $\langle \mu_z \rangle = \langle \psi_1^\pm | g_J J_z | \psi_1^\pm \rangle = 1.4\,\mu_B$/Ce, which is larger than the value obtained from the saturated magnetization. The positive value of λ^{ab} is consistent with ferromagnetic coupling between spins within the basal plane, while the smaller negative λ^c is consistent with weaker antiferromagnetic coupling between Ce layers.

B. Field dependence of the magnetic properties

To determine the behavior of the magnetic ground state in magnetic fields and to map the field-temperature phase diagrams, measurements of the specific heat and magnetization were performed in different applied fields. Figure 5(a) displays the low-temperature specific heat of CePdGa$_6$ with different fields applied along the c axis. Here, T_N is gradually suppressed with increasing field, and at fields >2 T, no magnetic transition is observed. Instead, there is a broad hump in C/T, which shifts to higher temperature with increasing field, corresponding to the Schottky anomaly from the splitting of the ground state doublet in the applied field. In Fig. 5(b), C/T is displayed for fields within the ab plane, where the antiferromagnetic transition is more robust than for fields along the c axis, and the broad Schottky anomaly is only clearly resolved in a field of 12 T. The differences in the field dependence for the two different field directions are consistent with the low-temperature Ising anisotropy in CePdGa$_6$, where a smaller field along the easy c axis can bring the system to the spin-polarized state.

The low-temperature $\chi(T)$ in different applied fields are displayed in Fig. 6. For fields along the c axis, distinctly
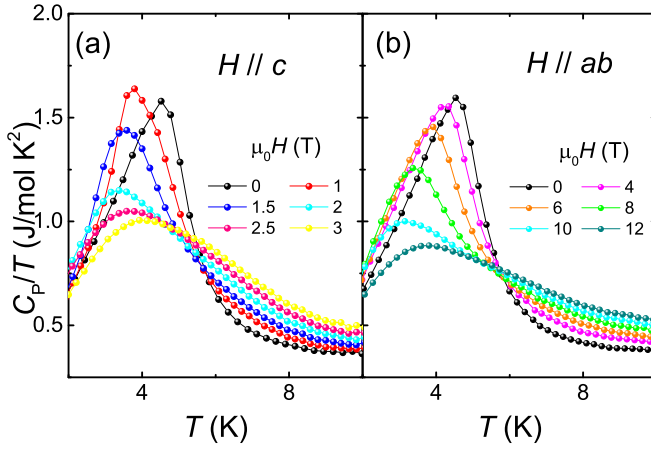
FIG. 5. Temperature dependence of the specific heat of CePdGa$_6$ in various applied magnetic fields (a) parallel to the c axis and (b) within the ab plane.

different behaviors are observed for different field ranges. In a field of 0.1 T, there is a sharp peak at T_N, corresponding to entering the antiferromagnetic ground state. At a larger field of 0.5 T, only a small hump is observed at T_N, while at low temperatures, there is an increase in $\chi(T)$, and at higher fields, there is broad peak which is gradually suppressed with field. Meanwhile, for fields within the ab plane up to at least 8 T, there is a gradual suppression of T_N, in line with the specific heat results.

The isothermal magnetization as a function of field along the c axis at three temperatures below T_N is displayed in Fig. 7(a), measured upon both sweeping the field up and down. In zero field, there is no remanent magnetization, consistent with a purely antiferromagnetic ground state. At 2 K, there are two metamagnetic transitions at $H_{m1} = 0.4$ T and $H_{m2} = 2.1$ T, where hysteresis is also observed, indicating a first-order nature; otherwise, the magnetization plateaus, with only a weak change of the magnetization with field. This is consistent with H_{m1} and H_{m2} corresponding to spin-flip
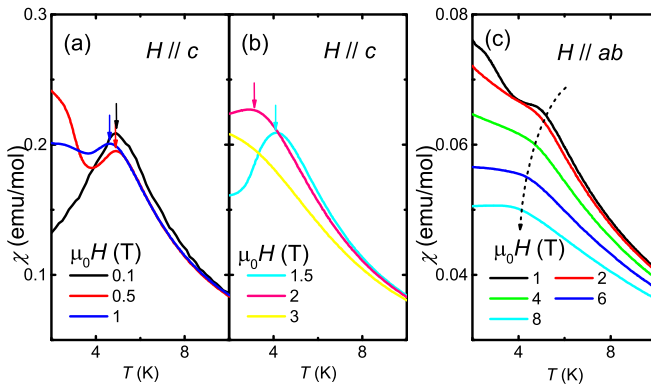

FIG. 7. (a) Isothermal field dependence of the magnetization $M(H)$ of CePdGa$_6$ for fields along the c axis, at three temperatures below T_N. The lower inset displays the low-field region of the data in the main panel, demonstrating hysteresis about the metamagnetic transition, while the upper inset shows $M(H)$ at 2 K for fields within the ab plane. (b) Field dependence of the resistivity $\rho(H)$ of CePdGa$_6$ at several temperatures for fields along the c axis. The dashed lines show the evolution of the two metamagnetic transitions.

transitions, with the spins remaining oriented along the c axis. For fields above H_{m2}, no magnetic transition is observed in the specific heat, and therefore, this likely corresponds to the system reaching the spin-polarized state, with a saturation magnetization of $M_s = 1.1\,\mu_B$/Ce. On the other hand, above H_{m1}, the magnetization reaches a value of $0.35\,\mu_B$/Ce, corresponding to $\approx M_s/3$, indicating a change of magnetic structure with a ferromagnetic component. While there is little change in the field dependence of the magnetization at 3 K, the curves at 4 K are drastically different. Instead of there being abrupt steplike metamagnetic transitions, the magnetization smoothly increases with field, reaching a very similar saturation value. This suggests that, at higher temperatures, the spins continuously rotate upon increasing the applied field rather than undergoing abrupt spin-flip transitions. The field-dependent magnetization at 2 K for fields in the ab plane is also shown in the inset of Fig. 7(a), which smoothly changes with field, with no sign of saturation up to at least 5 T, consistent with this being the hard direction of magnetization. The metamagnetic transitions are also revealed in the field dependence of the resistivity $\rho(H)$, as displayed in Fig. 7(b) for fields along the c axis. At 0.3 K, two abrupt anomalies are observed corresponding to H_{m1} and H_{m2}, which are also detected at 1.8 and 3 K. Above these transitions, there is a decrease of $\rho(H)$, consistent with the reduced spin-flip

FIG. 6. Temperature dependence of the magnetic susceptibility $\chi(T)$ of CePdGa$_6$ in different magnetic fields parallel to the c axis for fields (a) below and (b) above 1 T. The vertical arrows mark the position of the antiferromagnetic transition. (c) $\chi(T)$ for various fields applied within the ab plane, where the dashed line shows the evolution of T_N with field.
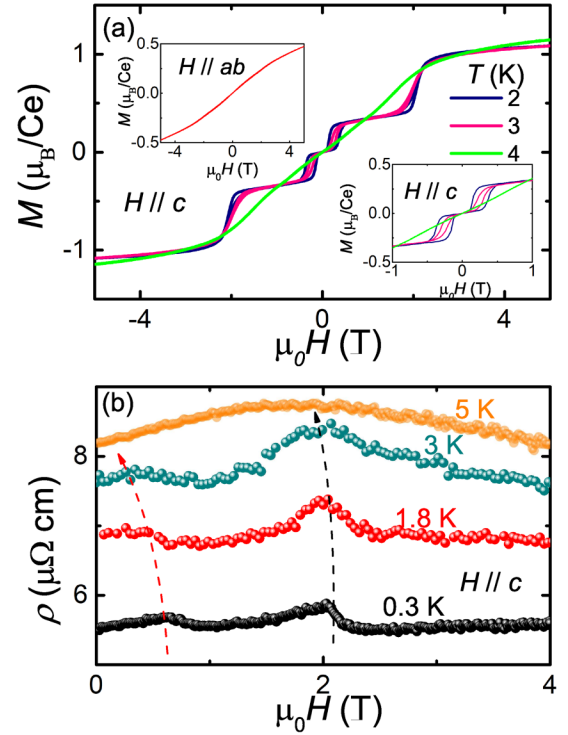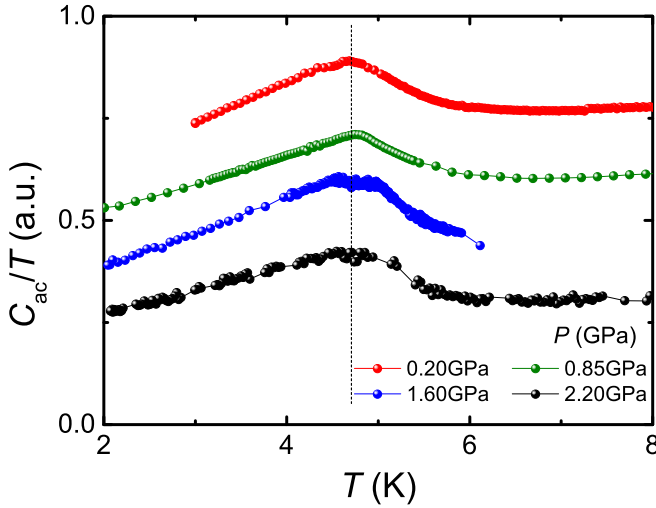
FIG. 8. Temperature dependence of the ac heat capacity of CePdGa$_6$ at various hydrostatic pressures up to 2.2 GPa. The vertical dashed line shows the position of the ambient pressure T_N, which remains nearly unchanged with pressure.

scattering arising from a larger ferromagnetic component to the magnetism. On the other hand, no metamagnetic transitions are detected at 5 K, where instead there is a broad peak in $\rho(H)$, again consistent with a more gradual reorientation of the spins with field at higher temperatures.

C. Magnetism of CePdGa$_6$ under pressure

To determine the evolution of the magnetic order under pressure, the temperature dependence of the ac specific heat of CePdGa$_6$ was measured at several different hydrostatic pressures up to 2.2 GPa, which are displayed in Fig. 8. It can be seen from the dotted line that there is little change of T_N with pressure, indicating the robustness of magnetic order. In the case of the layered Ce$_2$MGa$_{12}$ compounds, the T_N of Ce$_2$NiGa$_{12}$ and Ce$_2$PdGa$_{12}$ decrease with pressure, and antiferromagnetism is suppressed entirely >5.5 and 7 GPa, respectively [26,27]. On the other hand the T_N of Ce$_2$IrGa$_{12}$ undergoes a moderate enhancement from 3.1 to 3.7 K for pressures up to 2.3 GPa, indicating that this compound is located on the left side of the Doniach phase diagram [25]. In the case of CePdGa$_6$, the robustness of T_N suggests that measurements to higher pressures are required to situate this compound within the framework of the Doniach phase diagram and to examine whether there is pressure-induced quantum criticality in CePdGa$_6$.

IV. DISCUSSION

Our measurements of the resistivity, magnetic susceptibility, and specific heat show that CePdGa$_6$ orders antiferromagnetically below $T_N = 5.2$ K, with the moments oriented along the c axis. Figure 9 displays the temperature-field phase diagram for magnetic fields applied along the c axis. The phase boundaries obtained from different measurements are highly consistent, showing that T_N shifts to lower temperatures with field, before abruptly disappearing in a field of 2 T. At low temperatures, there are two steplike metamagnetic
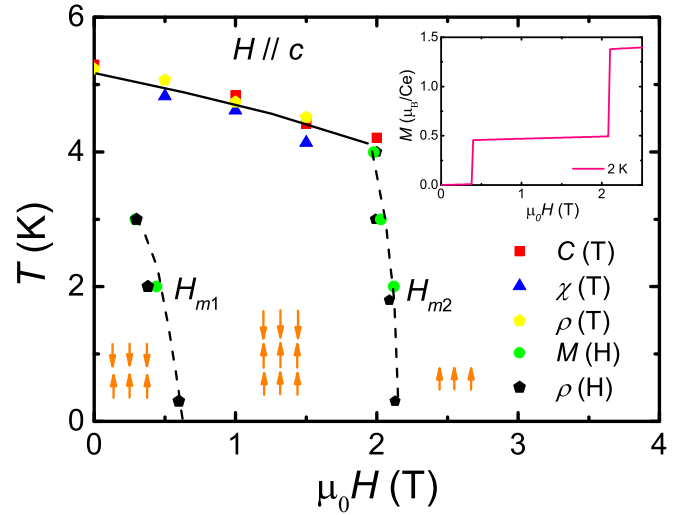

FIG. 9. Temperature-field phase diagram of CePdGa$_6$ at ambient pressure for fields along the easy c axis, from measurements of the resistivity, magnetization, and specific heat. The solid line shows the evolution of T_N, while the dashed lines show the positions of the low-temperature metamagnetic transitions. The magnetic structures at low temperature are also illustrated by the orange arrows where, in zero field, there is an antiferromagnetic ground state, while upon applying a field, the system passes through an intermediate $\uparrow\uparrow\downarrow$ phase before entering the spin-polarized state. The inset shows the field dependence of the magnetization based on mean-field calculations of the magnetic ground state calculated using the MᴄPʜᴀꜱᴇ software package [35], with the parameters described in the text.

transitions shown by the dashed lines, where the second transition is to the spin-polarized state, while the lower transition corresponds to a change of magnetic state to a phase with a magnetization of 0.35 μ_B/Ce, about one-third of the saturated value. Such steplike changes in the magnetization suggest that the spins are strongly constrained along the c axis, and therefore, there are abrupt spin-flip transitions for fields applied along the ordering direction. On the other hand, at 4 K, the magnetization changes smoothly with field, reaching the same saturated magnetization, indicating that, at this temperature, the spins continuously rotate in the applied field. Such a change with temperature may be a consequence of only a moderate magnetocrystalline anisotropy, as also evidenced by the relatively small value of the spin-wave gap $\Delta_{SW}/T_N \approx 0.4$ as compared with the other heavy-fermion gallides Ce$_2$IrGa$_{12}$ and Ce$_2$PdGa$_{12}$, which have Δ_{SW}/T_N of 1.5 and 2.8, respectively [24,25].

From the analysis of the magnetic susceptibility including the CEF contribution, the molecular field parameter is positive in the ab plane (λ^{ab}), while a smaller negative value is obtained along the c axis (λ^c). Together with the fact that only a relatively small field along the c axis is required to reach the spin-polarized state, this suggests that the antiferromagnetic ground state consists of ferromagnetically ordered Ce layers coupled antiferromagnetically along the c axis. The simplest model for such a system would consist of ferromagnetic Heisenberg exchange interactions between nearest neighbor Ce atoms within the ab plane $\mathcal{J}_0 > 0$ and antiferromagnetic exchange interactions $\mathcal{J}_1 < 0$ between nearest neighboring

layers as well as a sufficiently strong Ising anisotropy. This yields an *A*-type antiferromagnetic ground state consisting of ferromagnetic layers with moments orientated along the *c* axis, where the moment direction alternates between adjacent layers ↑↓↑↓. This model, however, cannot account for the field-induced phase with one-third magnetization since, for fields along the *c* axis, only a metamagnetic transition directly from the ↑↓↑↓ phase to the spin-polarized state is anticipated.

To realize the intermediate field-induced phase, it is necessary to consider an antiferromagnetic exchange $\mathcal{J}_2$ between next-nearest neighboring layers. In this case, from considering the classical ground state energies with sufficiently strong Ising anisotropy, the same ↑↓↑↓ ground state is realized for $\mathcal{J}_1/\mathcal{J}_2 > 2$, while a ↑↑↓↓ state occurs for $\mathcal{J}_1/\mathcal{J}_2 < 2$ [36]. Upon applying a magnetic field along the *c* axis, there is a metamagnetic transition at a field H_{m1} to an ↑↑↓ state with a net magnetization one-third of the saturated value and another at H_{m2} to the spin-polarized state, where H_{m2}/H_{m1} is determined by $\mathcal{J}_1/\mathcal{J}_2$. We performed mean-field calculations of the magnetic ground state and magnetization using the MCPHASE software package [35], which determines the most stable magnetic structure at a given temperature and magnetic field from considering multiple random starting moment configurations. These considered the Heisenberg exchange interactions described above as well as the CEF Hamiltonian $\mathcal{H}_{CF}$ with our deduced values of the Stevens parameters. As shown in the inset of Fig. 9, the observed values of $H_{m1} = 0.4$ T and $H_{m2} = 2.1$ T, from the midpoints of the metamagnetic transitions at 2 K, are well reproduced from the mean-field calculations at 2 K with $\mathcal{J}_1 = -0.023$ meV and $\mathcal{J}_2 = -0.0085$ meV, where for $H_{m1} < H < H_{m2}$, the ↑↑↓ ground state has the lowest energy. Keeping these values fixed, we find that a nearest neighbor in-plane ferromagnetic interaction $\mathcal{J}_0 = 0.034$ meV can yield the observed value of $T_N = 5.2$ K. Therefore, our analysis suggests stronger in-plane ferromagnetic interactions, where the value of $4\mathcal{J}_0/(2\mathcal{J}_1 + 2\mathcal{J}_2) = 2.16$ is close to our fitted value of $\lambda^{ab}/\lambda^c = 2.3$. Note that, here, we have assumed a ↑↓↑↓ ground state with $\mathcal{J}_1/\mathcal{J}_2 > 2$. Although a ↑↑↓↓ phase has been reported in CeCoGe$_3$ [37], such a scenario is less likely in CePdGa$_6$ due to the larger interlayer distances.

Compared with the layered heavy-fermion antiferromagnet CeRhIn$_5$, the magnetism in CePdGa$_6$ appears to have a much more three-dimensional character, whereas it is rather two-dimensional in the former, with $\mathcal{J}_1/\mathcal{J}_0 = 0.13$ deduced from inelastic neutron scattering [38]. In addition, in CeRhIn$_5$, the easy plane anisotropy and presence of in-plane antiferromagnetic interactions give rise to spiral magnetic order which is incommensurate along the *c* axis [13,14], and these features may be important factors for realizing the unconventional quantum criticality and superconductivity. On the other hand, the T_N of CePdGa$_6$ is much more robust with pressure, remaining almost unchanged at pressures up to 2.2 GPa.

Therefore an understanding of the relationship between the magnetism and any quantum critical behaviors will require measurements at considerably higher pressures.

In addition, despite the layered arrangement of Ce atoms, the *local* environment of the Ce atoms is relatively three dimensional, as evidenced by the derived CEF parameters being close to that for a cubic system (where $B_2^0 = 0$ and $|B_4^4| = 5|B_4^0|$). This CEF scheme can correctly predict the low-temperature Ising anisotropy, but the predicted moment along the *c* axis is larger than that observed. While such a reduced moment compared with that predicted from the CEF level scheme is often observed in heavy-fermion antiferromagnets due to screening of the moments by the Kondo effect [14,16,37,39,40], confirming whether such a scenario is applicable to CePdGa$_6$ requires a more precise determination of the CEF parameters, by measurements such as inelastic neutron scattering.

V. CONCLUSIONS

In summary, we have characterized the magnetic properties of the heavy-fermion antiferromagnet CePdGa$_6$ and their evolution upon the application of magnetic fields and pressure. We have constructed the temperature-field phase diagram for fields along the *c* axis where, at low temperatures, there are two abrupt metamagnetic transitions corresponding to spin-flip transitions. From the analysis of the magnetic susceptibility, we propose a CEF level scheme for the splitting of the ground state $J = \frac{5}{2}$ multiplet, indicating that the Ising anisotropy at low temperatures is driven by the sizable B_4^0 parameter. Moreover, our results are consistent with an antiferromagnetic ground state consisting of ferromagnetically coupled Ce layers, with antiferromagnetic coupling between layers. We have proposed a model for the exchange interactions which can explain the evolution of the magnetic ordering with applied magnetic field, which has sizable nearest neighbor and next-nearest neighbor layer interactions, indicating the presence of significant long-range magnetic interactions. Despite evidence for heavy-fermion behavior, there is negligible change of T_N upon applying pressures up 2.2 GPa, and hence, measurements at much higher pressures are necessary to look for evidence of quantum criticality.

[1] Z. Weng, M. Smidman, L. Jiao, X. Lu, and H. Q. Yuan, Multiple quantum phase transitions and superconductivity in Ce-based heavy fermions, Rep. Prog. Phys. **79**, 094503 (2016).

[2] Q. Si and F. Steglich, Heavy fermions and quantum phase transitions, Science **329**, 1161 (2010).

[3] P. Coleman, Heavy fermions: Electrons at the edge of magnetism, in *Handbook of Magnetism and Advanced Magnetic Materials*, edited by H. Kronmüller, S. Parkin, M. Fähnle, S. Maekawa, and I. Zutic (John Wiley and Sons, Ltd., Hoboken, 2007).

[4] S. Doniach, The Kondo lattice and weak antiferromagnetism, Physica B+C **91**, 231 (1977).

[5] N. Mathur, F. Grosche, S. Julian, I. Walker, D. Freye, R. Haselwimmer, and G. Lonzarich, Magnetically mediated superconductivity in heavy fermion compounds, Nature (London) **394**, 39 (1998).

[6] J. D. Thompson and Z. Fisk, Progress in heavy-fermion superconductivity: Ce115 and related materials, J. Phys. Soc. Jpn. **81**, 011002 (2012).

[7] T. Park, F. Ronning, H. Q. Yuan, M. B. Salamon, R. Movshovich, and J. D. Thompson, Hidden magnetism and quantum criticality in the heavy fermion superconductor $CeRhIn_5$, Nature (London) **440**, 65 (2006).

[8] C. Petrovic, P. G. Pagliuso, M. F. Hundley, R. Movshovich, J. L. Sarrao, J. D. Thompson, Z. Fisk, and P. Monthoux, Heavy-fermion superconductivity in $CeCoIn_5$ at 2.3 K, J. Phys.: Condens. Matter **13**, L337 (2001).

[9] A. L. Cornelius, P. G. Pagliuso, M. F. Hundley, and J. L. Sarrao, Field-induced magnetic transitions in the quasi-two-dimensional heavy-fermion antiferromagnets Ce_nRhIn_{3n+2} ($n = 1$ or 2), Phys. Rev. B **64**, 144411 (2001).

[10] G. Chen, S. Ohara, M. Hedo, Y. Uwatoko, K. Saito, M. Sorai, and I. Sakamoto, Observation of superconductivity in heavy-fermion compounds of Ce_2CoIn_8, J. Phys. Soc. Jpn. **71**, 2836 (2002).

[11] D. Kaczorowski, A. P. Pikul, D. Gnida, and V. H. Tran, Emergence of a Superconducting State from an Antiferromagnetic Phase in Single Crystals of the Heavy Fermion Compound Ce_2PdIn_8, Phys. Rev. Lett. **103**, 027003 (2009).

[12] M. Nicklas, V. A. Sidorov, H. A. Borges, P. G. Pagliuso, C. Petrovic, Z. Fisk, J. L. Sarrao, and J. D. Thompson, Magnetism and superconductivity in Ce_2RhIn_8, Phys. Rev. B **67**, 020506(R) (2003).

[13] N. J. Curro, P. C. Hammel, P. G. Pagliuso, J. L. Sarrao, J. D. Thompson, and Z. Fisk, Evidence for spiral magnetic order in the heavy fermion material $CeRhIn_5$, Phys. Rev. B **62**, R6100(R) (2000).

[14] W. Bao, P. G. Pagliuso, J. L. Sarrao, J. D. Thompson, Z. Fisk, J. W. Lynn, and R. W. Erwin, Incommensurate magnetic structure of $CeRhIn_5$, Phys. Rev. B **62**, R14621(R) (2000).

[15] W. Bao, P. G. Pagliuso, J. L. Sarrao, J. D. Thompson, Z. Fisk, and J. W. Lynn, Magnetic structure of heavy-fermion Ce_2RhIn_8, Phys. Rev. B **64**, 020401(R) (2001).

[16] A. D. Christianson, J. M. Lawrence, P. G. Pagliuso, N. O. Moreno, J. L. Sarrao, J. D. Thompson, P. S. Riseborough, S. Kern, E. A. Goremychkin, and A. H. Lacerda, Neutron scattering study of crystal fields in $CeRhIn_5$, Phys. Rev. B **66**, 193102 (2002).

[17] D. S. Christovam, C. Giles, L. Mendonca-Ferreira, J. Leão, W. Ratcliff, J. W. Lynn, S. Ramos, E. N. Hering, H. Hidaka, E. Baggio-Saitovich, Z. Fisk, P. G. Pagliuso, and C. Adriano, Spin rotation induced by applied pressure in the Cd-doped Ce_2RhIn_8 intermetallic compound, Phys. Rev. B **100**, 165133 (2019).

[18] J. Pelleg, G. Kimmel, and D. Dayan, RGa_6 (R = rare earth atom), a common intermetallic compound of the R-Ga systems, J. Less-Common Met. **81**, 33 (1981).

[19] E. Lidström, R. Wäppling, O. Hartmann, M. Ekström, and G. M. Kalvius, A μSR and neutron scattering study of $REGa_6$, where RE = Ce, Nd, Gd and Tb, J. Phys.: Condens. Matter **8**, 6281 (1996).

[20] R. T. Macaluso, J. N. Millican, S. Nakatsuji, H. O. Lee, B. Carter, N. O. Moreno, Z. Fisk, and J. Y. Chan, A comparison of the structure and localized magnetism in Ce_2PdGa_{12} with the heavy fermion $CePdGa_6$, J. Solid State Chem. **178**, 3547 (2005).

[21] J. Y. Cho, J. N. Millican, C. Capan, D. A. Sokolov, M. Moldovan, A. B. Karki, D. P. Young, M. C. Aronson, and J. Y. Chan, Crystal growth, structure, and physical properties of Ln_2MGa_{12} (Ln = La, Ce; M = Ni, Cu), Chem. Mater. **20**, 6116 (2008).

[22] S. Nallamuthu, T. P. Rashid, V. Krishnakumar, C. Besnard, H. Hagemann, M. Reiffers, and R. Nagalakshmi, Anisotropic magnetic, transport and thermodynamic properties of novel tetragonal Ce_2RhGa_{12} compound, J. Alloys Compd. **604**, 379 (2014).

[23] O. Sichevych, C. Krellner, Y. Prots, Y. Grin, and F. Steglich, Physical properties and crystal chemistry of Ce_2PtGa_{12}, J. Phys.: Condens. Matter **24**, 256006 (2012).

[24] D. Gnida and D. Kaczorowski, Magnetism and weak electronic correlations in Ce_2PdGa_{12}, J. Phys.: Condens. Matter **25**, 145601 (2013).

[25] Y. J. Zhang, B. Shen, F. Du, Y. Chen, J. Y. Liu, H. Lee, M. Smidman, and H. Q. Yuan, Structural and magnetic properties of antiferromagnetic Ce_2IrGa_{12}, Phys. Rev. B **101**, 024421 (2020).

[26] N. Kawamura, R. Sasaki, K. Matsubayashi, N. Ishimatsu, M. Mizumaki, Y. Uwatoko, S. Ohara, and S. Watanabe, High pressure properties for electrical resistivity and Ce valence state of heavy-fermion antiferromagnet Ce_2NiGa_{12}, J. Phys.: Conf. Ser. **568**, 042015 (2014).

[27] S. Ohara, T. Yamashita, T. Shiraishi, K. Matsubayashi, and Y. Uwatoko, Pressure effects on electrical resistivity of heavy-fermion antiferromagnet Ce_2PdGa_{12}, J. Phys.: Conf. Ser. **400**, 042048 (2012).

[28] R. T. Macaluso, S. Nakatsuji, H. Lee, Z. Fisk, M. Moldovan, D. Young, and J. Y. Chan, Synthesis, structure, and magnetism of a new heavy-fermion antiferromagnet, $CePdGa_6$, J. Solid State Chem. **174**, 296 (2003).

[29] H. Hegger, C. Petrovic, E. G. Moshopoulou, M. F. Hundley, J. L. Sarrao, Z. Fisk, and J. D. Thompson, Pressure-Induced Superconductivity in Quasi-2D $CeRhIn_5$, Phys. Rev. Lett. **84**, 4986 (2000).

[30] B. E. Light, R. S. Kumar, A. L. Cornelius, P. G. Pagliuso, and J. L. Sarrao, Heat capacity studies of Ce and Rh site substitution in the heavy-fermion antiferromagnet $CeRhIn_5$: Short-range magnetic interactions and non-Fermi-liquid behavior, Phys. Rev. B **69**, 024419 (2004).

[31] P. G. Pagliuso, N. O. Moreno, N. J. Curro, J. D. Thompson, M. F. Hundley, J. L. Sarrao, Z. Fisk, A. D. Christianson, A. H. Lacerda, B. E. Light, and A. L. Cornelius, Ce-site dilution studies in the antiferromagnetic heavy fermions

Ce$_m$Rh$_n$In$_{3m+2n}$ ($m = 1, 2; n = 0, 1$), Phys. Rev. B **66**, 054433 (2002).

[32] S. de Medeiros, M. Continentino, M. Orlando, M. Fontes, E. Baggio-Saitovitch, A. Rosch, and A. Eichler, Quantum critical point in CeCo(Ge$_{1-x}$Si$_x$)$_3$: Oral presentation, Phys. B: Condens. Matter **281**, 340 (2000).

[33] M. T. Hutchings, Point-charge calculations of energy levels of magnetic ions in crystalline electric fields, Solid State Phys. **16**, 227 (1964).

[34] J. Jensen and A. R. Mackintosh, *Rare Earth Magnetism: Structures and Excitations* (Oxford University Press, Oxford, 1991).

[35] M. Rotter, Using MCPHASE to calculate magnetic phase diagrams of rare earth compounds, J. Magn. Magn. Mater. **272**, E481 (2004).

[36] B. Li, Y. Sizyuk, N. S. Sangeetha, J. M. Wilde, P. Das, W. Tian, D. C. Johnston, A. I. Goldman, A. Kreyssig, P. P. Orth, R. J. McQueeney, and B. G. Ueland, Antiferromagnetic stacking of ferromagnetic layers and doping-controlled phase competition in Ca$_{1-x}$Sr$_x$Co$_{2-y}$As$_2$, Phys. Rev. B **100**, 024415 (2019).

[37] M. Smidman, D. T. Adroja, A. D. Hillier, L. C. Chapon, J. W. Taylor, V. K. Anand, R. P. Singh, M. R. Lees, E. A. Goremychkin, M. M. Koza, V. V. Krishnamurthy, D. M. Paul, and G. Balakrishnan, Neutron scattering and muon spin relaxation measurements of the noncentrosymmetric antiferromagnet CeCoGe$_3$, Phys. Rev. B **88**, 134416 (2013).

[38] P. Das, S.-Z. Lin, N. J. Ghimire, K. Huang, F. Ronning, E. D. Bauer, J. D. Thompson, C. D. Batista, G. Ehlers, and M. Janoschek, Magnitude of the Magnetic Exchange Interaction in the Heavy-Fermion Antiferromagnet CeRhIn$_5$, Phys. Rev. Lett. **113**, 246403 (2014).

[39] O. Stockert, E. Faulhaber, G. Zwicknagl, N. Stüßer, H. S. Jeevan, M. Deppe, R. Borth, R. Küchler, M. Loewenhaupt, C. Geibel, and F. Steglich, Nature of the *A* Phase in CeCu$_2$Si$_2$, Phys. Rev. Lett. **92**, 136401 (2004).

[40] E. A. Goremychkin and R. Osborn, Crystal-field excitations in CeCu$_2$Si$_2$, Phys. Rev. B **47**, 14280 (1993).